Transiently changing shape of the photon number distribution in a quantum-dot–cavity system driven by chirped laser pulses

M. Cosacchi,[1] T. Seidelmann,[1] F. Ungar,[1] M. Cygorek,[2] A. Vagov,[1,3] and V. M. Axt[1]
[1]*Theoretische Physik III, Universität Bayreuth, D-95440 Bayreuth, Germany*
[2]*Department of Physics, University of Ottawa, Ottawa, Ontario, Canada K1N 6N5*
[3]*ITMO University, St. Petersburg, 197101, Russia*

(Received 10 March 2020; revised manuscript received 24 April 2020; accepted 28 April 2020; published 13 May 2020)

We have simulated the time evolution of the photon number distribution in a semiconductor quantum-dot–microcavity system driven by chirped laser pulses and compare with unchirped results. When phonon interactions with the dot are disregarded—thus corresponding to the limit of atomic cavity systems—chirped pulses generate photon number distributions that change their shape drastically in the course of time. Phonons have a strong and qualitative impact on the photon statistics. The asymmetry between phonon absorption and emission destroys the symmetry of the photon distributions obtained for positive and negative chirps. While for negative chirps transient distributions resembling thermal ones are observed, for positive chirps the photon number distribution still resembles its phonon-free counterpart but with overall smoother shapes. In sharp contrast, using unchirped pulses of the same pulse area and duration wave packets are found that move up and down the Jaynes-Cummings ladder with a bell shape that changes little in time. For shorter pulses and lower driving strength Rabi-like oscillations occur between low photon number states. For all considered excitation conditions transitions between sub- and super-Poissonian statistics are found at certain times. For resonant driving with low intensity the Mandel parameter oscillates and is mostly negative, which indicates a nonclassical state in the cavity field. Finally, we show that it is possible that the Mandel parameter dynamically approaches zero and still the photon distribution exhibits two maxima and thus is far from being a Poissonian.

DOI: 10.1103/PhysRevB.101.205304

I. INTRODUCTION

Semiconductor quantum-dot–cavity (QDC) systems continue to raise attention as highly integrable on-demand emitters of nonclassical states of light. In particular, QDCs have proven to be rather successful providing, e.g., reliable on-demand high quality single photon sources [1–10] as well as sources for entangled photon pairs [11–18]. Clearly, QDCs support a much larger class of excitations when higher mean photon numbers are reached. The additional degrees of freedom provided by higher number photon states obviously allow for a rich variety of dynamical scenarios and may open the way to new kinds of applications such as, e.g., the encoding of quantum information in the photon number state distribution. These possibilities are, however, far from being explored.

Often, the first step to characterize systems with photon distributions ranging up to higher photon numbers is to record a few characteristic numbers such as the mean photon number [19] and/or the Mandel parameter [20]. In simple cases, the mean photon number is indeed enough to capture the whole information about the photon distribution even when the latter is time dependent. This applies in particular when photons are generated by classically driving an empty cavity without a quantum dot (QD) where the photonic system is at all times in a coherent state and thus the distribution is a Poissonian [21,22], i.e., in this case the photonic excitation is always as close as possible to a classical light field and thus nonclassical states cannot be reached. Moreover, although the mean photon number varies in time, the photon distribution keeps its shape at all times.

The situation is different when a system with few discrete levels near resonance to a cavity mode such as an atom or a quantum dot is placed inside the cavity. When driving transitions between these discrete levels deviations from the coherent state may occur as is evident, e.g., by monitoring the Mandel parameter,

$$Q(t) = (\langle \Delta n^2 \rangle - \langle n \rangle)/\langle n \rangle. \tag{1}$$

$Q(t)$ measures the deviation of the mean-square fluctuation from the mean photon number normalized to the latter. Therefore, Q vanishes for a Poisson distribution. A positive Q indicates a super-Poissonian distribution with larger fluctuations than in a coherent state with the same mean photon number while negative Q values correspond to the sub-Poissonian regime which is known to have no classical analog [23]. Indeed, deviations from the coherent state have been reported for the stationary distribution obtained in an atomic cavity with constant driving where different signs of Q have been found for different ratios between cavity loss and radiative decay rates [24]. In Ref. [25] it has been shown that the statistics of photons emitted from the exciton-biexciton system of a QD can be steered from sub- to the super-Poissonian by varying the biexciton binding energy, the pump strength or the temperature [26]. Although the experiments in

Ref. [25] have been performed on QDs without cavity, the number of modes in the theoretical modeling was restricted to two which corresponds to the situation in a QDC. Therefore, the results should also apply to QDCs. Simulations for a pulsed excitation of a QDC indicate that Q can exhibit oscillations and change its sign repeatedly in time [27].

It is clear, however, that in general the photon number distribution contains much more detailed information than captured by the mean photon number or the Mandel parameter. Recently, calculations of the stationary photon number distribution in a constantly driven QDC revealed a strong qualitative influence of phonons on the shape of the distribution [28,29]. While without phonons distributions with many different shapes were found for different detunings, the stationary distribution with phonons turned out to be close to a thermal state with a high effective temperature. Note that the case without phonons describes, e.g., a cavity with a trapped atom.

Advances in measuring techniques have demonstrated possibilities for observing directly the photon number resolved distributions in various systems without the necessity to perform quantum tomography to reconstruct the entire state [30], ranging from bimodal microlasers [31] over QDs [32,33] to exciton-polariton condensates [34]. Furthermore, a novel algorithm for data evaluation free of systematic errors to obtain number distributions has been successfully employed [35]. These achievements could pave the way to novel applications where easy access to information encoded in the photon number distribution is needed.

The focus of the present paper is on the transient behavior of the photon number distribution in a QDC system driven by chirped pulses in comparison to the unchirped case. Our most striking result is the finding that the shape of the number distribution changes dynamically when driving the QDC with chirped pulses. In sharp contrast, for sufficiently strong unchriped excitations a wave packet which keeps a bell shape for all times moves up and down the Jaynes-Cummings ladder. Phonons have noticeable effects on the photon statistics for all excitation conditions that we compare. Notably, for chirped excitation the phonon impact induces qualitative changes of the shape of the distribution in particular for negative chirps.

II. THEORY

A. Model and methods

We study a self-assembled QD, e.g., GaAs/In(Ga)As, with strong electronic confinement, such that only the lowest conduction and the highest valence band states need to be taken into account. Furthermore, we consider only situations where the system is well represented by a two-level model. The latter applies, e.g., for resonant driving of the exciton by circularly polarized light when the fine-structure splitting is negligible or when all other states such as the biexciton are sufficiently far from resonance. Then the Hamiltonian for the laser driven dot reads

$$H_{\mathrm{DL}} = -\hbar\Delta\omega_{\mathrm{LX}}|X\rangle\langle X| - \frac{\hbar}{2}f(t) \times \left(e^{-i\varphi(t)}|X\rangle\langle G| + e^{i\varphi(t)}|G\rangle\langle X|\right), \tag{2}$$

where the detuning between the exciton and central laser frequency $\Delta\omega_{\mathrm{LX}} := \omega_{\mathrm{L}} - \omega_{\mathrm{X}}$ is introduced. Here, the ground state $|G\rangle$ is chosen as the zero of the energy scale. Note that the usual dipole and rotating wave approximations are employed and the Hamiltonian is written down in a frame co-rotating with the laser frequency ω_{L}. The real amplitude $f(t)$ and the phase $\varphi(t)$ are related to the instantaneous Rabi frequency $\Omega(t)$ by

$$\Omega(t) := 2\mathbf{M_0}\cdot\mathbf{E}(t) = f(t)\,e^{-i(\omega_{\mathrm{L}}t+\varphi(t))}, \tag{3}$$

where $\mathbf{M_0}$ is the dipole matrix element of the transition between the QD ground $|G\rangle$ and exciton state $|X\rangle$ and $\mathbf{E}$ is the positive frequency part of the laser field.

To enhance the coupling between the QD and the electromagnetic field, the dot can be placed into a microcavity. We account for a single cavity mode with frequency ω_{C} far from the electromagnetic continuum and a QD coupled to that mode close to resonance via

$$H_{\mathrm{C}} = \hbar\Delta\omega_{\mathrm{CL}}a^\dagger a + \hbar g\left(a^\dagger|G\rangle\langle X| + a|X\rangle\langle G|\right), \tag{4}$$

where the cavity photons are created (annihilated) by the bosonic operator $a^\dagger$ (a) and are detuned by $\Delta\omega_{\mathrm{CL}} := \omega_{\mathrm{C}} - \omega_{\mathrm{L}}$ from the laser frequency. The QD is coupled to the cavity with a strength of $\hbar g$.

The subsystem of interest comprising the dot laser and the cavity Hamiltonian H_{DL} and H_{C}, respectively, is not an ideal few-level system, since it is embedded into the surrounding solid-state matrix. Even at cryogenic temperatures of a few Kelvin, the QD exciton is prone to the coupling to phonons. In strongly confined excitonic systems, the most important phononic contribution usually results from the deformation potential coupling to longitudinal acoustic (LA) phonons and is of the elastic pure dephasing type [36–39],

$$H_{\mathrm{Ph}} = \hbar\sum_{\mathbf{q}}\omega_{\mathbf{q}}b_{\mathbf{q}}^\dagger b_{\mathbf{q}} + \hbar\sum_{\mathbf{q}}\left(\gamma_{\mathbf{q}}^{\mathrm{X}}b_{\mathbf{q}}^\dagger + \gamma_{\mathbf{q}}^{\mathrm{X}*}b_{\mathbf{q}}\right)|X\rangle\langle X|, \tag{5}$$

where the bosonic operator $b_{\mathbf{q}}^\dagger$ ($b_{\mathbf{q}}$) creates (destroys) phonons with frequency $\omega_{\mathbf{q}}$. $\gamma_{\mathbf{q}}^{\mathrm{X}}$ denotes the coupling constant between the exciton state and the bosonic mode labeled by its wave vector $\mathbf{q}$ which is adequate for bulk phonons. Here, we use the fact that in GaAs/In(Ga)As the lattice properties of the dot and its surroundings are similar, such that phonon confinement is negligible. Other QD-phonon interaction mechanisms like, e.g., the piezoelectric coupling to LA and transverse acoustic (TA) phonons can become important in strongly polar crystals such as, e.g., GaN-based QDs [40,41], but are of minor importance for GaAs-type structures.

Finally, we account for Markovian loss processes by phenomenological decay rates for the radiative decay and cavity losses, respectively, that are incorporated into the model as Lindblad-type superoperators $\mathcal{L}_{|G\rangle\langle X|,\gamma}\bullet + \mathcal{L}_{a,\kappa}\bullet$ with

$$\mathcal{L}_{O,\Gamma}\bullet = \Gamma\left(O\bullet O^\dagger - \frac{1}{2}\{\bullet, O^\dagger O\}_+\right), \tag{6}$$

where $\{\cdot,\cdot\}_+$ denotes the anticommutator. O is a system operator and Γ the decay rate of the associated loss process, i.e., in our case γ stands for the radiative decay rate while κ is the cavity loss rate.

The dynamical equation to be solved is the Liouville-von Neumann equation for the density matrix,

$$\frac{\partial}{\partial t}\rho = -\frac{i}{\hbar}\{H, \rho\}_- + \mathcal{L}_{|G\rangle\langle X|,\gamma}\rho + \mathcal{L}_{a,\kappa}\rho, \tag{7}$$

with the total Hamiltonian $H = H_{\mathrm{DL}} + H_{\mathrm{C}} + H_{\mathrm{Ph}}$ and $\{\cdot,\cdot\}_-$ denotes the commutator.

We employ a path-integral formalism for simulating the dynamics in the above-defined model in a numerically complete fashion. By tracing out the phonon degrees of freedom analytically, a non-Markovian memory kernel decaying on a time scale of a few picoseconds is obtained that manifests in experiments as, e.g., non-Lorentzian line shapes in linear and nonlinear spectra [37,38,42,43] or in characteristic dependencies of the phonon-induced damping of Rabi rotations [44–47]. Therefore, this memory cannot be neglected in calculating the QD dynamics which takes place on a similar time scale. We call a numerical solution complete if a finer time discretization or a longer cutoff of the phonon-induced memory kernel does not change the results noticeably.

Most current implementations of the real-time path-integral approach are based on the pioneering work of Makri and Makarov [48,49], who introduced an iterative scheme for the augmented density matrix of the subsystem of interest. We are using an extension of this scheme that allows the inclusion of non-Hamiltonian Lindblad-type contributions into the path-integral algorithm without the loss of precision with respect to the phonon-induced part of the dynamics by formulating the iterative scheme not in a Hilbert, but a Liouville space [50]. In the present study, the system that couples to the phonons is represented by a large number of basis states of the form $|G, n\rangle$ and $|X, n\rangle$ where n denotes the photon number and G or X indicates whether the dot is in its ground or excited state. A numerically complete study of such systems is currently impossible with the Makri-Makarov algorithm due to the extreme growth of the numerical demand with rising number of system states. Nevertheless, we are able to present numerically complete results because we are using a recently developed reformulation of the algorithm that iterates a partially summed augmented density matrix [28]. Note that this reformulation of the path-integral algorithm does not introduce any additional approximations. For details on the methods, consider the supplement of Ref. [28]. The photon number distribution is obtained by taking the corresponding matrix element of the subsystem's reduced density operator $\bar{\rho} = \mathrm{Tr}_{\mathrm{Ph}}[\rho]$, with $\mathrm{Tr}_{\mathrm{Ph}}$ denoting the trace over the phonon degrees of freedom,

$$P_n(t) = \sum_{\nu=\mathrm{G,X}} \langle \nu, n|\bar{\rho}(t)|\nu, n\rangle. \tag{8}$$

B. Chirped pulses and laser-dressed states

In order to generate a chirped pulse one usually starts with a Gaussian pulse with an envelope and phase:

$$f_0(t) = \frac{\Theta}{\sqrt{2\pi}\sigma} e^{-\frac{(t-t_0)^2}{2\sigma^2}}, \tag{9}$$

$$\varphi(t) = \mathrm{const.}, \tag{10}$$

where Θ denotes the pulse area and σ determines the duration corresponding to a full width at half maximum (FWHM) of $\mathrm{FWHM} = 2\sqrt{2\ln(2)}\sigma$ and t_0 marks the time of the pulse maximum. We shall assume in the following a resonant excitation where $\varphi(t) = 0$ in Eq. (3) for an unchirped pulse. We note in passing that also other pulse shapes are possible as a starting point for the generation of chirped pulses. In particular, secant hyperbolic pulses may have advantages in certain circumstances [51].

Passing the initial pulse in Eq. (9) through a Gaussian chirp filter [52] yields a chirped pulse with envelope and phase:

$$f_{\mathrm{chirp}}(t) = \frac{\Theta_{\mathrm{chirp}}}{\sqrt{2\pi}\sigma_{\mathrm{chirp}}} e^{-\frac{(t-t_0)^2}{2\sigma_{\mathrm{chirp}}^2}}, \tag{11}$$

$$\varphi(t) = a\,(t-t_0)^2/2, \tag{12}$$

pulse area $\Theta_{\mathrm{chirp}} = \Theta\sqrt{\sigma_{\mathrm{chirp}}/\sigma}$ and duration $\sigma_{\mathrm{chirp}} = \sqrt{(\alpha^2/\sigma^2) + \sigma^2}$. The phase in Eq. (3) has acquired a quadratic time dependence, which corresponds to an instantaneous laser frequency $\omega_{\mathrm{L}} + \dot{\varphi} = \omega_{\mathrm{L}} + a\,(t - t_0)$ that changes linearly in time and for $\omega_{\mathrm{L}} = \omega_{\mathrm{X}}$ crosses the exciton resonance at the pulse maximum $t = t_0$. The strength of the chirp is commonly expressed in terms of the chirp parameter α which is related to the coefficient a in Eq. (12) by $a = \alpha/(\alpha^2 + \sigma^4)$. Note that the pulse area and in particular the pulse length increases drastically when chirps are introduced (cf. the definition of σ_{chirp}).

III. NUMERICAL RESULTS ON TRANSIENT PHOTON STATISTICS

For the numerical calculations, we assume a QD with 6-nm diameter and standard GaAs parameters [28,41]. The cavity is coupled to the QD exciton with a strength of $\hbar g = 0.1$ meV while it is on resonance, i.e., $\Delta\omega_{\mathrm{CX}} := \omega_{\mathrm{C}} - \omega_{\mathrm{X}} = 0$. The cavity losses are taken to be $\hbar\kappa = 6.6\,\mu$eV, which corresponds to a quality factor $\approx 10^5$ assuming a mode frequency of $\hbar\omega_{\mathrm{C}} = 1.5$ eV. The radiative decay rate of the QD exciton is set to $\hbar\gamma = 2\,\mu$eV.

A. The chirp-free situation

Let us first concentrate on the chirp-free case. Figures 1(a) and 1(c) display photon number distributions at different times for a QDC driven by an unchirped Gaussian pulse with a pulse area of 5π and a duration of 2.4 ps FWHM. Figure 1(a) shows results without phonons while in Fig. 1(c) the corresponding simulations with phonons are depicted assuming the phonons before the pulse to be in thermal equilibrium at a temperature of T = 4 K. The initial state for the cavity photons is taken to be the vacuum, i.e., the $n = 0$ Fock state and the QD is initially in the ground state.

As expected the photons stay in the vacuum state until the arrival of the pulse. At the end of the 5π pulse (cf. black markers in Fig. 1) the QD is in the exciton state and the resonant coupling to the cavity initiates vacuum Rabi oscillations [53–57], i.e., oscillations between the $|X, n = 0\rangle$ and the $|G, n = 1\rangle$ states. This is reflected in the photon distribution as oscillations between the $n = 0$ and $n = 1$ Fock states and results in damped oscillations of the mean photon number

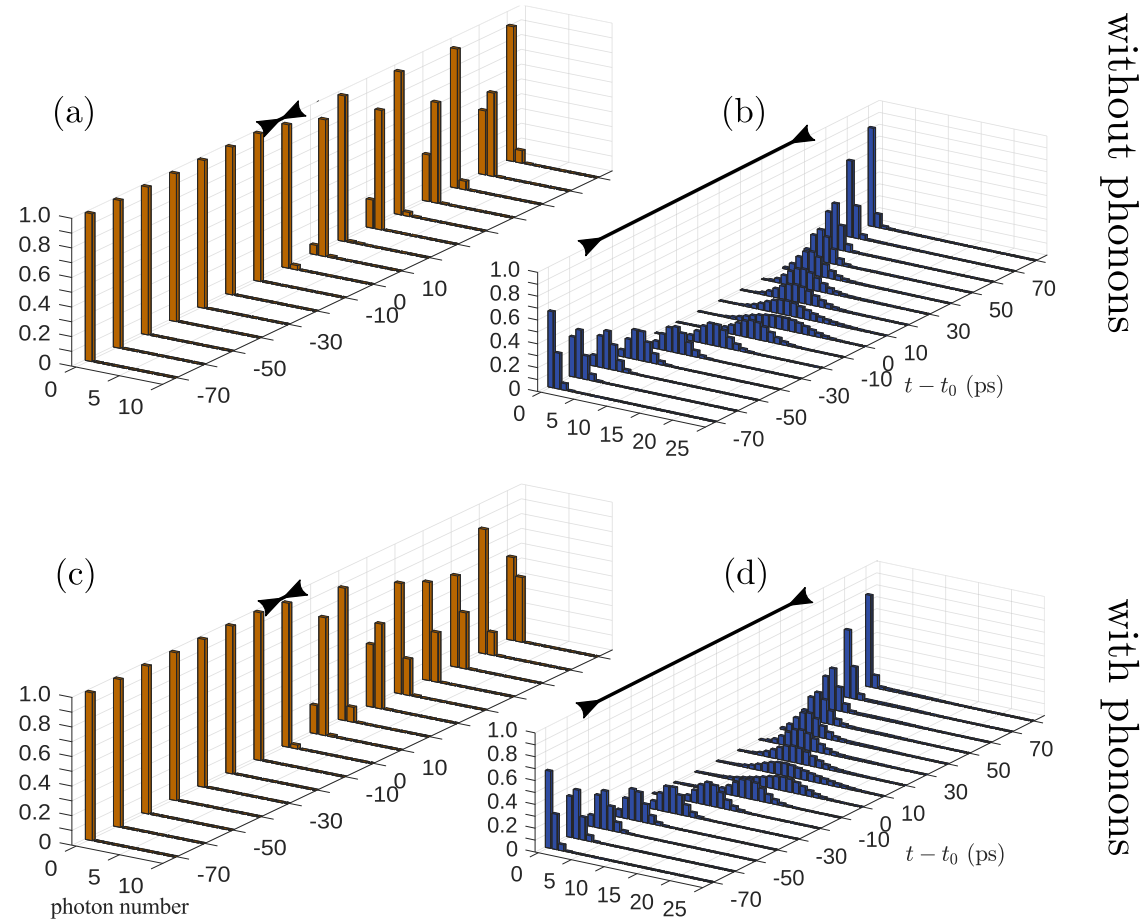

FIG. 1. Transient photon number distributions for laser excitations with unchirped pulses with (a) and (c) pulse area $\Theta = 5\pi$ and duration FWHM=2.4 ps, (b) and (d) pulse area $\Theta = 31.63\pi$ and duration FWHM $= 94.22$ ps. Panels (c) and (d) display results accounting for phonons that are initially at equilibrium at a temperature of $T = 4$ K while the corresponding phonon-free results are shown in (a) and (b). The pulse has its maximum at $t = t_0$. Black markers indicate the FWHM of the pulse.

between zero and and a maximal amplitude that due to losses and phonon effects is below one [cf. orange curve in Fig. 3(a)]. Quantitatively, a small occupation of the two-photon state $|2\rangle$ is observed, seen, e.g., for $t - t_0 = 10$ ps in Figs. 1(a) and 1(c). The reason lies in the re-excitation of the QD during the same pulse, whereby effectively two photons can be put into the single cavity mode.

The phonon impact on Rabi-type oscillations in a two-level system has been extensively studied [29,44–47,58–64] and shall therefore not be analyzed here in detail. We just note that the main effects are a phonon-induced damping, which depends on the driving strength, and a renormalization of the Rabi frequency. The renormalization of g is reflected in Figs. 1(a) and 1(c) by slightly different oscillation frequencies. The damping seen in the orange curve in Fig. 3(a) is the result of the combined effects of phonons, cavity losses, and radiative decay.

For a fair comparison between unchirped and chirped pulses, recall that the application of a Gaussian chirp filter involves besides the time-dependent variation of the phase $\varphi(t)$ in Eq. (12) also a considerable increase of the pulse duration and of the pulse area. Therefore, we show in Figs. 1(b) and 1(d) the photon distribution with and without the influence of phonons for a pulse with pulse area $\Theta = 31.63\pi$ and duration FWHM $= 94.22$ ps, which corresponds to the application of a filter with an effective value of $|\alpha| = 40$ ps^2 in Eq. (11) but keeping the phase $\varphi(t) = 0$ constant. Most strikingly, with this driving there are no traces of vacuum Rabi oscillations visible. Instead, a wave-packet-type dynamics sets in, where a bell-shaped distribution is found for all times. The mean photon number rises monotonically in time to values $n \approx 12$ [note that the blue curve in Fig. 3(a) is scaled down by a factor of 5 for better visibility] and subsequently falls back to zero after the pulse has vanished.

B. Finite chirps

Figure 2 displays transient photon number distributions obtained for chirped pulses that are generated by passing the Gaussian pulse used in Figs. 1(a) and 1(c) through a chirp filter with $\alpha = \pm 40$ ps^2 [(a) and (c) $\alpha = -40$ ps^2, (b) and (d) $\alpha = +40$ ps^2]. The upper panels correspond to simulations without phonons while for the lower panels the interaction with phonons has been included. Note that the pulses used in Fig. 2 have the same pulse area and duration as the unchirped pulses used in Figs. 1(b) and 1(d) which allows us to compare excitation conditions where the only difference is the frequency modulation.

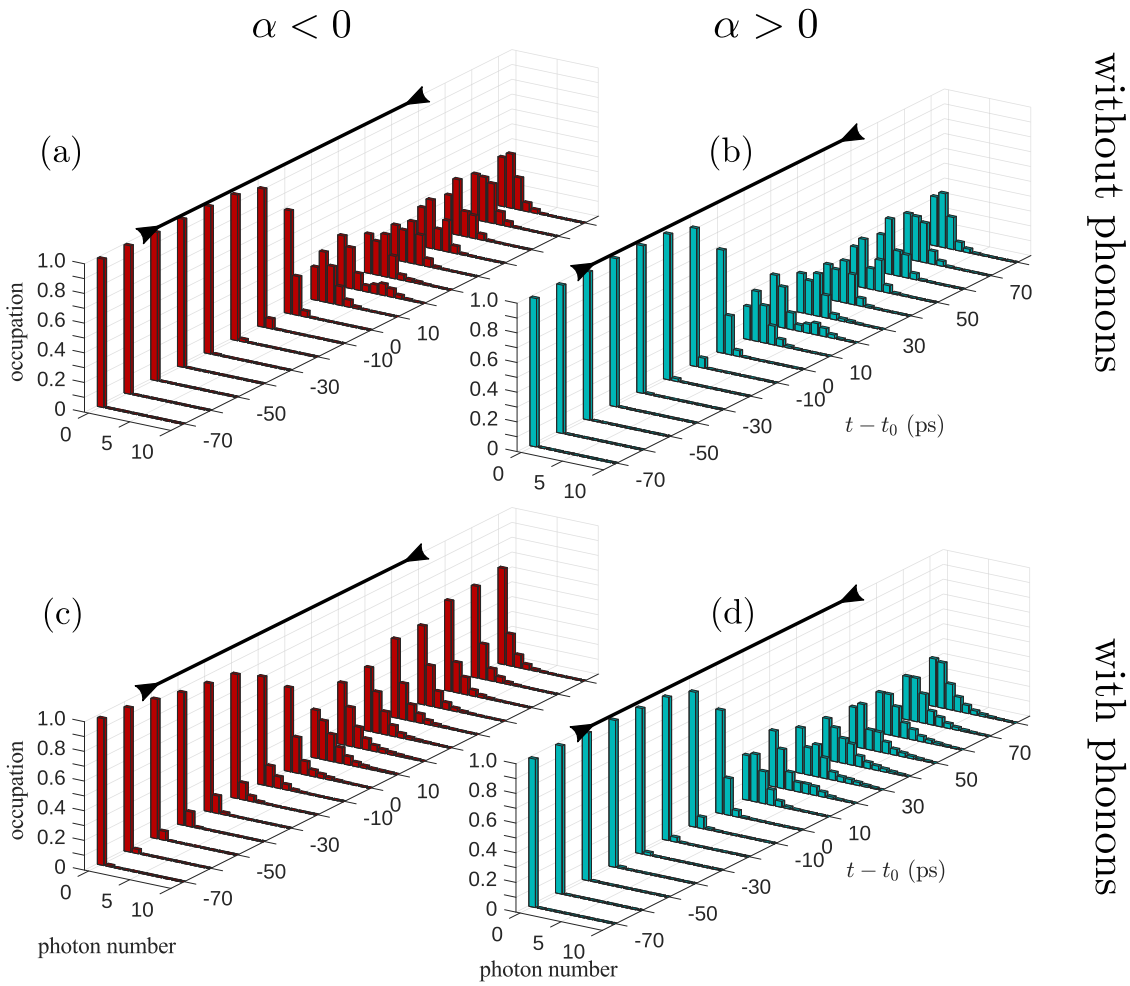

FIG. 2. Transient photon number distributions for laser excitations with chirped pulses with pulse area and FWHM before the chirp filter of $\Theta = 5\pi$ and FWHM=2.4 ps, i.e., $\Theta_{\text{chirp}} = 31.63\pi$ and duration $\text{FWHM}_{\text{chirp}} = 94.22$ ps for $|\alpha| = 40$ ps^2. (a) and (c) Calculated with chirp parameter $\alpha = -40$ ps^2, (b) and (d) $\alpha = +40$ ps^2. (c) and (d) Displayed are results accounting for phonons that are initially at equilibrium at a temperature of $T = 4$ K while the corresponding phonon-free results are shown in (a) and (b). The pulse has its maximum at $t = t_0$. Black markers indicate the FWHM of the pulse after the chirp filter.

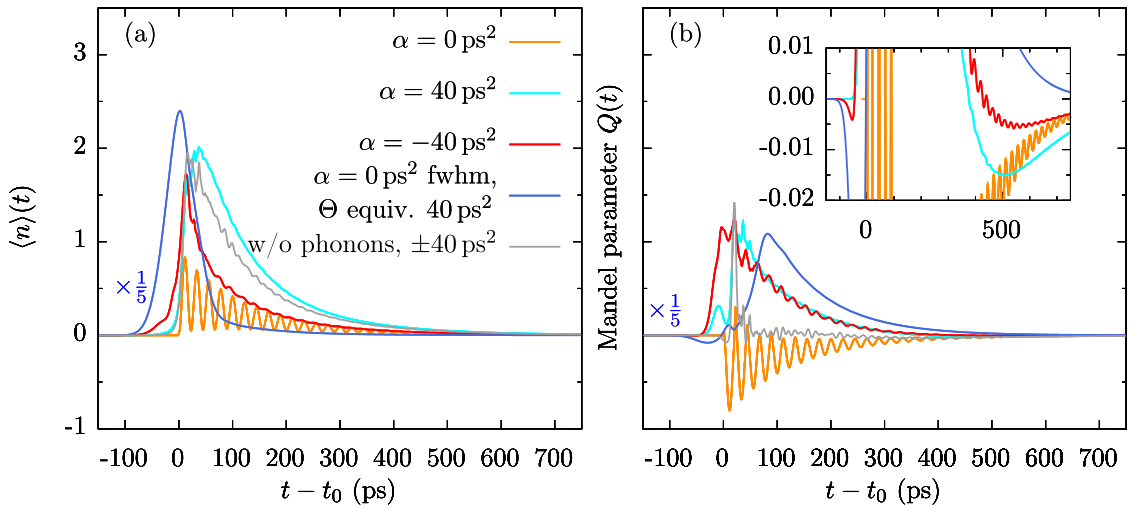

FIG. 3. The time-dependent (a) mean photon number and (b) Mandel parameter $Q(t) = (\langle \Delta n^2 \rangle - \langle n \rangle)/\langle n \rangle$ for the cases indicated by the labels. All curves are calculated with phonons initially at $T = 4$ K, except for the gray curves which correspond to the phonon-free case. The blue curve is scaled down by a factor of 5 for better visibility. The inset in (b) corresponds to a zoomed-in scale.

In the phonon-free case identical distributions are obtained for positive and negative chirp [cf. Figs. 2(a) and 2(b)]. This symmetry is removed when phonons are taken into account [cf. Figs. 2(c) and 2(d)]. In contrast to the unchirped case with the same pulse area and duration in Figs. 1(b) and 1(d), the photon number is close to zero until the pulse maximum is reached, which can be explained by noting that for chirped pulses the instantaneous laser frequency is strongly detuned from the QD resonance for times away from the pulse maximum. The most striking difference compared with Figs. 1(b) and 1(d) is, however, that the photon distributions in Fig. 2 significantly change their shape in time. The distributions found in the phonon free case have at early times after the pulse maximum a bell shape with a single maximum and transform into a bimodal distribution with two well-separated bell-shaped contributions at later times [cf. $t - t_0 = 20\,\mathrm{ps}$ in Fig. 2(a)]. Subsequently, at times $t - t_0 \approx 30-50\,\mathrm{ps}$ the distribution still has two peaks but looks rather jagged having little resemblance with bell-shaped distributions. Eventually, at later times only a single maximum is found which appears at a finite photon number or at zero, depending on time.

Phonons change the situation qualitatively for negative chirp [cf. Fig. 2(c)], where now the photon number distribution has a single maximum at $n = 0$ for all times. The shape of the transient distribution resembles thermal photon occupations, which due to mean photon numbers around $n = 2$ [cf. Fig. 3(a)] corresponds to an effective temperature above $T_{\mathrm{eff}} \approx 40\,000$ K for photon energies $\hbar\omega_{\mathrm{C}} \approx 1.5$ eV. A similar impact of phonons on the photon number distribution has been reported previously for the stationary distribution found at long times for permanent driving [28]. The phonon impact for positive chirp is less dramatic [cf. Fig. 2(d)]. As in the phonon-free case, there are still times where the distribution is bi-modal while at other times only a single maximum is found. Overall, the irregular looking shape appearing at certain times in Figs. 2(a) and 2(b) is smoothened. Moreover, there is a tendency to build up a maximum near $n = 0$.

Further differences between the number distributions in Figs. 1 and 2 are revealed by looking at the time evolution of the corresponding Mandel parameters $Q(t)$ in Fig. 3(b). For a Fock state the number fluctuation disappears, leading to a negative Mandel parameter, except for the $n = 0$ Fock state, where the Mandel parameter approaches an expression of the form zero divided by zero. We see from the orange curves in Fig. 3 that for weakly driven unchirped pulses the damped oscillation of the mean photon number between 0 and at most 1 is accompanied by damped oscillations of the Mandel parameter ranging down to almost -1 and up to essentially 0. The negative values of the minima correspond to times where the system is close to the $n = 1$ Fock state. If the dynamics would exclusively involve states with photon numbers 0 or 1 such that only P_0 and P_1 are different from zero, it is easy to show that for all times, where $P_1 \neq 0$, the Mandel parameter is $Q(t) = -\langle n\rangle$. Therefore, Q should approach 0 when the $n = 0$ Fock state is approached. We see, however, from the orange curve in Fig. 3(b) that the first maxima of the Mandel parameter Q are a bit above 0, indicating small admixtures of higher number states.

For higher pulse areas Q is positive for most of the time for chirped as well as for unchirped pulses. Interestingly, although the bell-shaped distributions in Figs. 1(b) and 1(d) at first glance resemble much more Poissonian distributions than the somehow irregular ones found for chirped pulses in Figs. 2(b) and 2(d) their deviation from a Poissonian as measured by the Mandel parameter is much larger than for chirped pulses [note that the blue curve in Fig. 3(b) is scaled down by a factor of 5]. But most remarkably, in the calculation with finite chirp without phonons [cf. the gray line in Fig. 3(b)] the Mandel parameter decays extremely fast after its initial rise to positive values compared with the other situations considered. Most notably, already at around $\sim$40 ps after the pulse maximum it has dropped close to zero. In sharp contrast to the common interpretation that a Mandel parameter near zero implies a distribution with a shape close to a Poissonian, Fig. 2(b) shows a jagged distribution with two maxima at $\sim$40 ps after the pulse maximum. Therefore, using the Mandel parameter as a measure for the deviation from a Poisonian is not valid in all physically relevant situations.

We further note that the Mandel parameter calculated for all excitation conditions studied in this paper changes its sign during the course of time. Without chirp and low intensities (orange curve) this happens near the first maxima of the Q oscillations, as discussed above, but also for higher driving strength (blue curve) a sign change occurs indicating that before the pulse maximum is reached the photon distribution is sub-Poissonian and switches at the pulse maximum to super-Poissonian. Also for the chirped excitations Q exhibits sign changes as revealed by the inset in Fig. 3(b). Actually, the Mandel parameter calculated for high pulse areas falls below zero before approaching its asymptotic value of zero from below for chirped as well as for unchirped excitations. Indeed, also the blue curve in Fig. 3(b) falls below zero at $t - t_0 = 1090\,\mathrm{ps}$ (not seen in the plotted range). This sign change of Q shortly before cavity losses have relaxed the photon distribution to the empty cavity, can be understood as follows. The maximal photon numbers that are transiently reached for high pulse areas are well above one. The cavity losses remove photons from the cavity such that eventually the limit of $n = 0$ with zero fluctuations is reached. However, since the cavity losses for a state with n photons scale like $\sim n$, the relaxation from states with $n > 1$ to lower states is faster than the final relaxation from the $n = 1$ to the $n = 0$ states. Therefore, before the final relaxation is completed the photons preferably occupy the $n = 1$ state which results in a negative Mandel parameter before the asymptotic value of zero is reached. Note that this effect presumes only $\kappa \neq 0$ and thus should be robust with respect to variations of this parameter.

Finally, we note that Q exhibits small amplitude oscillations for chirped pulses which are absent in the unchirped case. A similar but less pronounced tendency is seen in the mean photon number.

C. Interpretation in terms of laser-dressed states

A popular application of driving QDs with chirped laser pulses is the robust preparation of exciton or biexciton states by invoking an adiabatic rapid passage (ARP) process [65–75]. ARP exploits the adiabatic theorem of quantum mechanics which predicts a time evolution through instantaneous

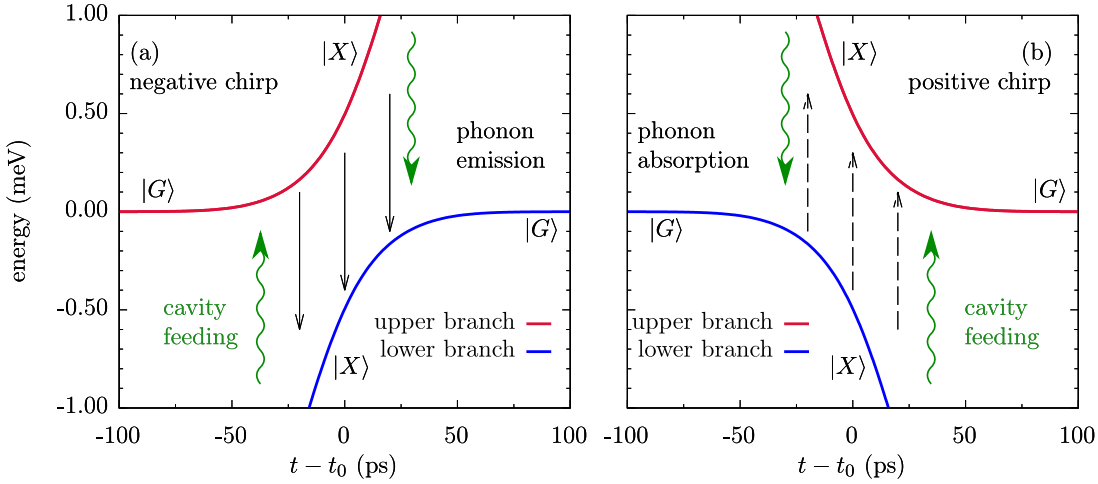

FIG. 4. Time evolution of the upper and lower laser-dressed state energies with respect to the excitation pulse maximum at $t = t_0$. While for negative chirps (a) phonon emission is probable (represented by black arrows), for positive chirps (b) phonon absorption is suppressed at low temperatures, which is indicated by the dashed arrows. Green curly arrows indicate transitions between laser-dressed states due to the QD cavity feeding.

eigenstates (dressed states) of the system provided the external driving fulfills the restrictions of the adiabatic regime [76]. In order to comply with these restrictions for a two-level system driven by Gaussian chirped pulses with a frequency modulation given by Eq. (12), it is advisable to transform the QD-laser Hamiltonian H_{DL} in Eq. (13) to a frame co-rotating with the phase φ to get rid of a possibly rapidly changing coupling. The transformed Hamiltonian reads

$$\widetilde{H}_{\mathrm{DL}} = -\hbar(\Delta\omega_{\mathrm{LX}} + a\,(t - t_0))|X\rangle\langle X| - \frac{\hbar}{2} f(t)(|X\rangle\langle G| + |G\rangle\langle X|). \tag{13}$$

The laser-dressed states can now be defined as the instantaneous eigenstates of $\widetilde{H}_{\mathrm{DL}}$. The corresponding eigenenergies are plotted in Fig. 4, where the left panel corresponds to a negative chirp while the result for positive chirp is shown in the right panel. The distinctive feature of ARP is that when the system is in the ground state $|G\rangle$ long before the pulse (i.e., for $t \to -\infty$) it will evolve adiabatically towards the exciton state $|X\rangle$ after the pulse (i.e., for $t \to +\infty$) independent of the sign of the chirp. However, it is important to note that the evolution proceeds along the lower (upper) branch for positive (negative) chirp. This affects in particular the impact of phonons. In general phonons can efficiently induce transitions between the two branches. However, at low temperatures phonon absorption is strongly suppressed and phonon emission can invoke only transitions from the upper to the lower branch (cf. the black arrows in Fig. 4). That is why phonons have little effects on the ARP dynamics for positive chirp while for negative chirp the ARP-based exciton preparation is strongly disturbed [68,70,73,74]. In order to preserve an efficient exciton preparation also at negative chirps, it has been recently demonstrated that high pulse areas can be used since this effectively decouples the phonons from the electronic system [29,75].

When also a cavity is coupled to the QD, then the coupling leads to Rabi-type rotations between states $|X, n\rangle$ and $|G, n+1\rangle$ with different numbers n of cavity photons. In particular for times when the laser is far off-resonant and the laser-dressed states are close to the undressed states, the effect of coupling the QD to a cavity can be understood as inducing a transition between the dressed states similar to the coupling to phonons. To be a bit more specific, when the system is in the exciton state the QD-cavity coupling leads to a feeding of the cavity by an additional photon accompanied by a transition from the $|X\rangle$-like branch to the $|G\rangle$-like branch (cf. the green curly arrows in Fig. 4). At early times, the reverse process, where one photon disappears from the cavity while transferring the system from the ground to the exciton state is suppressed since there are initially no photons in the cavity.

We shall now try to interpret the pertinent features of the photon dynamics in some more detail using the simplified picture where the system evolves adiabatically through the laser-dressed states in Fig. 4 while phonons and cavity feeding induce transitions between these states.

In the case of a negative chirp [cf. Fig. 4(a)] transitions form the upper branch to the lower branch of the laser-dressed states accompanied by phonon emission are possible before and after the pulse maximum at $t = t_0$. Thus, phonons should have a profound impact on the resulting photon statistics during the entire pulse. In fact, this explains why the distribution is close to a thermal one at all times [cf. Fig. 2(c)]. For times before the pulse reaches its maximum, cavity feeding can occur form the excitonlike lower branch to the upper branch, which has a large ground-state contribution. Subsequently, the system can again decay to the lower branch by phonon emission followed by another cavity feeding process back into the upper branch and so on. Because of this constructive interplay between phonon and cavity feeding processes, higher photon states can be reached compared with the phonon-free situation for $t \leqslant t_0$ [cf. Figs. 2(a) and 2(c)]. In the time interval shortly after the pulse maximum the upper branch becomes the state with the excitonlike characteristics and cavity feeding now takes place from the upper branch into the ground-state-like lower branch of the laser-dressed states. Thus, after the pulse

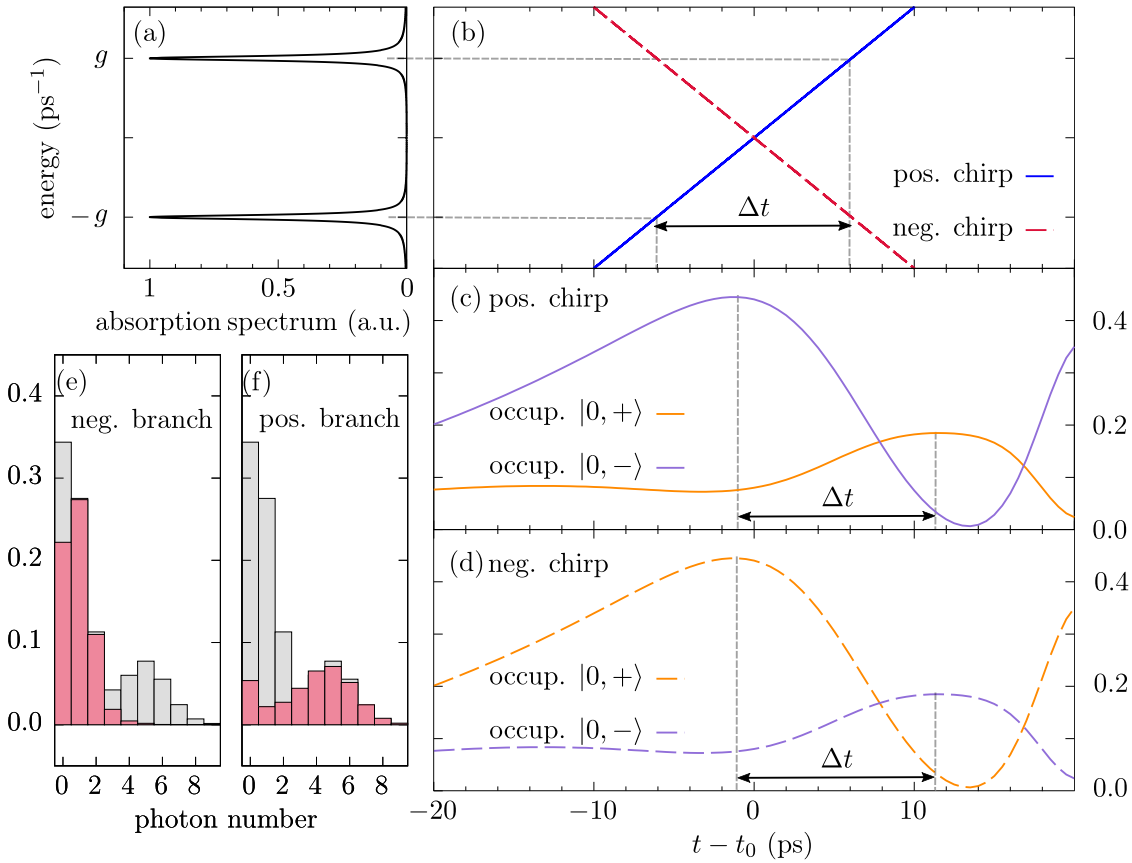

FIG. 5. (a) Linear absorption spectrum of the QDC system. (b) Time-dependent instantaneous frequency, blue (red) for positive (negative) chirp. Δt marks the time elapsed between the crossing of the two resonances. (c) and (d) Time evolution of the occupations of the lowest excited eigenstates of the QDC system [(c) for positive and (d) for negative chirp]. (e) and (f) Photon number distribution at $t - t_0 = 20$ ps (gray); red, accounting only for $|n,+\rangle$ (e) or $|n,-\rangle$ (f) states. Here, only phonon-free results are shown.

maximum has appeared phonon and cavity feeding processes are now in direct competition with each other. Therefore, compared with the phonon-free situation, the mean photon number should be reduced. Altogether, for negative chirp, the phonon impact on the photon distributions is visible at all times leading to nearly thermal distributions. At times before the pulse maximum the interaction with phonons increases the mean photon number because of a constructive interplay between phonon and cavity feeding processes. This effect is reversed after the pulse maximum and the mean photon number is reduced compared with the phonon-free situation due to the phonon interaction, as can be seen comparing the red with the gray curve in Fig. 3(a).

The situation is different when the chirp is positive as seen in Figs. 2(b) and 2(d). Here, a phonon influence on the photon statistics can be hardly seen before the pulse maximum. This can again be explained by inspection of the branches of the laser-dressed states. Starting in the ground state the system evolves adiabatically alongside the lower branch. Since phonon absorption processes are suppressed at low temperatures, transitions to the excitonlike upper state are unlikely to occur. Also cavity feeding is hardly possible [cf. Fig. 4(b)] and, like in the phonon-free situation, the system remains essentially in the ground state without photons and phonons have almost no visible effect. This observation changes after the pulse maximum. Now, cavity feeding processes accompanied by transitions from the excitonlike lower branch to the upper branch appear. Subsequently, phonon emission processes take place, resulting in a transition back to the lower branch. Thus, now, a constructive interplay between phonon emission and cavity feeding is possible, leading to a thermalization of the photon distribution. Therefore, after a transition time of a few 10 ps the distribution resembles a thermal distribution. Because of the constructive interplay the mean photon number is increased compared with the phonon-free situation, as can be seen comparing the cyan with the gray curve in Fig. 3(a). Consequently, only for a finite time interval after the pulse maximum photon distributions can be detected which are similar to the distributions in the phonon-free situation and display irregular behavior or several maxima.

D. Interpretation in terms of cavity-dressed states

Finally, we would like to explain why chirped pulse excitation leads to photon number distributions where the number of maxima changes dynamically from one to two and back to one. To this end we have to go beyond the laser-dressed state picture and recall that the linear absorption of a QDC comprises two lines split by $\Delta\omega = 2g$ [cf. Fig. 5(a)]. Thus, the instantaneous frequency of a pulse with positive chirp first crosses the energetically lower resonance and then, delayed

by a time $\Delta t = 2g/a$, the higher one [cf. Fig. 5(b)]. Each crossing of these resonances initiates a wave packet climbing up the Jaynes-Cummings ladder. This behavior is efficiently described in the picture of the cavity-dressed states, i.e., the eigenstates of the dot-cavity Hamiltonian, which relate to the bare QD states by

$$|n,+\rangle = \frac{1}{\sqrt{2}}(+|X,n\rangle + |G,n+1\rangle),$$
$$|n,-\rangle = \frac{1}{\sqrt{2}}(-|X,n\rangle + |G,n+1\rangle), \tag{14}$$

in the case of a resonant cavity mode $\omega_X - \omega_C = 0$.

Starting from the state $|G,0\rangle$ only the two states $|0,\pm\rangle$ can be reached directly by the laser coupling and thus climbing up the Jaynes cummings ladder one has to pass these states. Since the corresponding eigenenergies are separated by $2g$, the transitions to these states are in resonance with the instantaneous frequency of a chirped pulse at different times. Indeed, Fig. 5(c) reveals that the occupation of the lowest excited eigenstate of the QDC system $|0,-\rangle$ rises before the upper state $|0,+\rangle$ acquires a noticeable occupation. The maximum occupation of $|0,-\rangle$ is reached ≈ 5 ps after the instantaneous frequency has crossed the lower resonance, revealing the reaction time of the system. $|0,+\rangle$ is maximally occupied delayed exactly by Δt from the maximal occupation of $|0,-\rangle$. The time ordering of the excitation of the $|0,\pm\rangle$ states is reversed when reversing the sign of the chirp [cf. Fig. 5(d)] since now the upper resonance is crossed first.

The laser driving couples $|n,+\rangle$ to $|n,-\rangle$ states. However, when the instantaneous frequency is in resonance with transitions between $|n,+\rangle$ states with adjacent n then the transitions to $|n,-\rangle$ states are off-resonant and vice versa. Thus, it can be expected that the packets running up the Jaynes-Cummings ladder are essentially composed either of $|n,+\rangle$ or $|n,-\rangle$ states. Indeed, this is confirmed by Figs. 5(e) and 5(f) which displays in gray the photon number distribution at time $t - t_0 = 20$ ps, i.e., the time where according to Fig. 2(b) the two maxima are most pronounced. Also shown in red are photon number distributions calculated according to

$$P_n^{(\pm)} = \begin{cases} \frac{1}{2}\left(\langle n,\pm|\rho|n,\pm\rangle + \langle n-1,\pm|\rho|n-1,\pm\rangle\right) \\ \quad \text{for } n > 0, \\ \frac{1}{2}\left(\langle 0,\pm|\rho|0,\pm\rangle + \langle G,0|\rho|G,0\rangle\right) \\ \quad \text{for } n = 0 \end{cases}. \tag{15}$$

Recalling that for a cavity in resonance with the QD transition the $|n,\pm\rangle$ states have a probability of $1/2$ for finding n or $n+1$ photons, Eq. (15) yields, for $n > 0$, the probability for having n photons when accounting only for either the $|n,+\rangle$ or the $|n,-\rangle$ states. For $n = 0$ the contribution from $|G,0\rangle$ is counted by $1/2$ for the plus and minus branch, since this state can be counted as lower or upper state. We note in passing that $P_n^{(-)}$ [red bars in Fig. 5(e)] does not add up with $P_n^{(+)}$ [red bars in Fig. 5(f)] to the total photon number P_n (gray bars in Fig. 5), because P_n comprises coherences between the $|n,+\rangle$ and the $|n,-\rangle$ states in addition to their occupations. Nevertheless, Fig. 5 reveals that the two peaks in the photon number distribution can be attributed unambiguously either to the upper or lower branch of the QDC states.

Altogether this explains the time evolution of the peaks in the photon number distribution. After crossing the first resonance the distribution has a single peak since at first only a single packet is climbing up the Jaynes-Cumming ladder. When the second resonance is crossed a second packet is initiated such that at $t - t_0 \approx 20$ ps two well-resolved packets are observed. Both packets move up and down the Jaynes-Cummings ladder similar to the single wave packet observed for the unchirped excitation in Figs. 1(b) and 1(d). Since the decline of the first packet starts while the second is still rising, at some time both packets overlap. Although the packets are no longer well resolved, two maxima are still found over an extended time period [30 ps $\lesssim t - t_0 \lesssim$ 50 ps in Fig. 2(b)]. At later times the relaxation drives both packets to low photon numbers such that the maxima merge and a single-peaked distribution is recovered.

Finally, we note that for a cavity in resonance with the QD transition the energies of the QDC eigenstates $|n,\pm\rangle$ are found in the rotating frame at $\hbar\omega_{n,\pm} = \pm g\sqrt{n+1}$ such that the transition energies between states with adjacent n are all different and decrease with rising n. Therefore, the instantaneous frequency of a chirped pulse crosses all of these resonances at different times which is likely to contribute to the somewhat irregular looking time evolution of the photon number distribution found in particular in the intermediate time interval 30 ps $\lesssim t - t_0 \lesssim$ 50 ps in Fig. 2(b).

IV. CONCLUSION

We have studied transient photon number distributions generated in a microcavity by a pulsed excitation of an embedded quantum dot. We find qualitatively different photon distributions for chirped and unchirped pulses. Phonons have a noticeable influence on the photon distributions in particular for negative chirps, where the phonon coupling introduces qualitative changes of the shape of the distribution already at a temperature of $T = 4$ K. To be more specific, phonons lead in this case to almost thermalized photon distributions at high effective temperatures for all times. For positive chirp, the transient distributions are far away from a thermal one for times after the pulse maximum until about 80 ps afterwards.

For all investigated cases, we find that the Mandel parameter changes its sign during the time evolution of the system, indicating the ability to enter and leave a regime of genuine nonclassical photon statistics in the course of time. Moreover, cases were encountered where the Mandel parameter is zero, but the photon number distribution has two peaks and is definitely not a Poissonian. Therefore, one has to be careful when using the Mandel parameter as a measure for the deviation from a Poissonian distribution, as it is often done [24,77–80]. This finding underlines the necessity to carefully consider the definition of the Mandel parameter, which indeed yields zero for a Poissonian distribution. But the reverse implication is obviously not true for all cases.

Our most striking result is, however, that the shape of the photon number distribution changes significantly during the time evolution when the system is excited by chirped pulses. In fact, when the excitation starts to populate states with higher photon numbers, one observes at first bell-shaped distributions with a single maximum that increases in time.

Subsequently, two well-separated bell-shaped contributions develop which at later times first evolve into a single broad feature with two peaks and eventually merge into a distribution with a single peak. This is in sharp contrast to the unchirped case, where for the same high driving strengths the photon number distributions keep a bell shape with a single maximum for all times. Our analysis reveals that the transient changes of the shape of the photon distribution in the chirped case can be attributed to subsequent crossings of resonances of the quantum-dot–cavity system by the instantaneous frequency.

We believe that our findings deepen the understanding of the transient behavior of photon distributions in a driven quantum-dot–cavity system and its dependence on the driving conditions. This might pave the way to targeted manipulations of photon distributions which could result in new types of photonic applications in the future.

ACKNOWLEDGMENTS

M.Cy. thanks the Alexander-von-Humboldt foundation for support through a Feodor Lynen fellowship. A.V. acknowledges the support from the Russian Science Foundation under Project No. 18-12-00429 which was used to study dynamical processes nonlocal in time by the path-integral approach. This work was also funded by the Deutsche Forschungsgemeinschaft (DFG, German Research Foundation) Project No. 419036043.

[1] P. Michler, A. Kiraz, C. Becher, W. V. Schoenfeld, P. M. Petroff, L. Zhang, E. Hu, and A. Imamoglu, Science **290**, 2282 (2000).
[2] C. Santori, M. Pelton, G. Solomon, Y. Dale, and Y. Yamamoto, Phys. Rev. Lett. **86**, 1502 (2001).
[3] C. Santori, D. Fattal, J. Vuckovic, G. S. Solomon, and Y. Yamamoto, Nature (London) **419**, 594 (2002).
[4] Y.-M. He, Y. He, Y.-J. Wei, D. Wu, M. Atatüre, C. Schneider, S. Höfling, M. Kamp, C.-Y. Lu, and J.-W. Pan, Nat. Nanotechnol. **8**, 213 (2013).
[5] Y.-J. Wei, Y.-M. He, M.-C. Chen, Y.-N. Hu, Y. He, D. Wu, C. Schneider, M. Kamp, S. Höfling, C.-Y. Lu, and J.-W. Pan, Nano Lett. **14**, 6515 (2014).
[6] X. Ding, Y. He, Z.-C. Duan, N. Gregersen, M.-C. Chen, S. Unsleber, S. Maier, C. Schneider, M. Kamp, S. Höfling, C.-Y. Lu, and J.-W. Pan, Phys. Rev. Lett. **116**, 020401 (2016).
[7] N. Somaschi, V. Giesz, L. De Santis, J. C. Loredo, M. P. Almeida, G. Hornecker, S. L. Portalupi, T. Grange, C. Antón, J. Demory, C. Gómez, I. Sagnes, N. D. Lanzillotti-Kimura, A. Lemaítre, A. Auffeves, A. G. White, L. Lanco, and P. Senellart, Nat. Photonics **10**, 340 (2016).
[8] L. Schweickert, K. D. Jöns, K. D. Zeuner, S. F. Covre da Silva, H. Huang, T. Lettner, M. Reindl, J. Zichi, R. Trotta, A. Rastelli, and V. Zwiller, Appl. Phys. Lett. **112**, 093106 (2018).
[9] L. Hanschke, K. A. Fischer, S. Appel, D. Lukin, J. Wierzbowski, S. Sun, R. Trivedi, J. Vučković, J. J. Finley, and K. Müller, npj Quantum Inf. **4** (2018).
[10] M. Cosacchi, F. Ungar, M. Cygorek, A. Vagov, and V. M. Axt, Phys. Rev. Lett. **123**, 017403 (2019).
[11] N. Akopian, N. H. Lindner, E. Poem, Y. Berlatzky, J. Avron, D. Gershoni, B. D. Gerardot, and P. M. Petroff, Phys. Rev. Lett. **96**, 130501 (2006).
[12] R. M. Stevenson, R. J. Young, P. Atkinson, K. Cooper, D. A. Ritchie, and A. J. Shields, Nature (London) **439**, 179 (2006).
[13] R. Hafenbrak, S. M. Ulrich, P. Michler, L. Wang, A. Rastelli, and O. G. Schmidt, New J. Phys. **9**, 315 (2007).
[14] A. Dousse, J. Suffczynski, A. Beveratos, O. Krebs, A. Lemaître, I. Sagnes, J. Bloch, P. Voisin, and P. Senellart, Nature (London) **466**, 217 (2010).
[15] E. del Valle, New J. Phys. **15**, 025019 (2013).
[16] M. Müller, S. Bounouar, K. D. Jöns, M. Glässl, and P. Michler, Nat. Photonics **8**, 224 (2014).
[17] A. Orieux, M. A. M. Versteegh, K. D. Jöns, and S. Ducci, Rep. Prog. Phys. **80**, 076001 (2017).
[18] T. Seidelmann, F. Ungar, A. M. Barth, A. Vagov, V. M. Axt, M. Cygorek, and T. Kuhn, Phys. Rev. Lett. **123**, 137401 (2019).
[19] Y. T. Chough and H. J. Carmichael, Phys. Rev. A **54**, 1709 (1996).
[20] L. Mandel, Opt. Lett. **4**, 205 (1979).
[21] C. Gerry and P. L. Knight, *Introductory Quantum Optics* (Cambridge University Press, Cambridge, 2004).
[22] Note that fields produced by lasers in real experiments usually have some degree of amplitude noise. Therefore, the photon number distribution is always a bit wider than the Poissonian one.
[23] W. Vogel and D.-G. Welsch, *Quantum Optics* (Wiley-VCH, Weinheim, 2006).
[24] T. Quang and H. Freedhoff, Phys. Rev. A **47**, 2285 (1993).
[25] G. Callsen, A. Carmele, G. Hönig, C. Kindel, J. Brunnmeier, M. R. Wagner, E. Stock, J. S. Reparaz, A. Schliwa, S. Reitzenstein, A. Knorr, A. Hoffmann, S. Kako, and Y. Arakawa, Phys. Rev. B **87**, 245314 (2013).
[26] Although the experiments in Ref. [25] have been performed on QDs without cavity, the number of modes in the theoretical modeling was restricted to two which corresponds to the situation in a QDC. Therefore, the results should also apply to QDCs.
[27] M. Bagheri Harouni, R. Roknizadeh, and M. H. Naderi, Phys. Rev. B **79**, 165304 (2009).
[28] M. Cygorek, A. M. Barth, F. Ungar, A. Vagov, and V. M. Axt, Phys. Rev. B **96**, 201201(R) (2017).
[29] D. E. Reiter, T. Kuhn, and V. M. Axt, Adv. Phys.: X **4**, 1655478 (2019).
[30] A. I. Lvovsky and M. G. Raymer, Rev. Mod. Phys. **81**, 299 (2009).
[31] E. Schlottmann, M. von Helversen, H. A. M. Leymann, T. Lettau, F. Krüger, M. Schmidt, C. Schneider, M. Kamp, S. Höfling, J. Beyer, J. Wiersig, and S. Reitzenstein, Phys. Rev. Appl. **9**, 064030 (2018).
[32] M. Schmidt, M. von Helversen, M. López, F. Gericke, E. Schlottmann, T. Heindel, S. Kück, S. Reitzenstein, and J. Beyer, J. Low Temp. Phys. **193**, 1243 (2018).
[33] M. v. Helversen, J. Böhm, M. Schmidt, M. Gschrey, J.-H. Schulze, A. Strittmatter, S. Rodt, J. Beyer, T. Heindel, and S. Reitzenstein, New J. Phys. **21**, 035007 (2019).
[34] M. Klaas, E. Schlottmann, H. Flayac, F. Laussy, F. Gericke, M. Schmidt, M. Helversen, J. Beyer, S. Brodbeck, H. Suchomel,

S. Höfling, S. Reitzenstein, and C. Schneider, Phys. Rev. Lett. **121**, 047401 (2018).
[35] J. Hloušek, M. Dudka, I. Straka, and M. Ježek, Phys. Rev. Lett. **123**, 153604 (2019).
[36] L. Besombes, K. Kheng, L. Marsal, and H. Mariette, Phys. Rev. B **63**, 155307 (2001).
[37] P. Borri, W. Langbein, S. Schneider, U. Woggon, R. L. Sellin, D. Ouyang, and D. Bimberg, Phys. Rev. Lett. **87**, 157401 (2001).
[38] B. Krummheuer, V. M. Axt, and T. Kuhn, Phys. Rev. B **65**, 195313 (2002).
[39] V. M. Axt, T. Kuhn, A. Vagov, and F. M. Peeters, Phys. Rev. B **72**, 125309 (2005).
[40] I. A. Ostapenko, G. Hönig, S. Rodt, A. Schliwa, A. Hoffmann, D. Bimberg, M. R. Dachner, M. Richter, A. Knorr, S. Kako, Y. Arakawa, Phys. Rev. B **85**, 081303(R) (2012).
[41] B. Krummheuer, V. M. Axt, T. Kuhn, I. D'Amico, and F. Rossi, Phys. Rev. B **71**, 235329 (2005).
[42] A. Vagov, V. M. Axt, T. Kuhn, W. Langbein, P. Borri, and U. Woggon, Phys. Rev. B **70**, 201305(R) (2004).
[43] D. E. Reiter, Phys. Rev. B **95**, 125308 (2017).
[44] J. Förstner, C. Weber, J. Danckwerts, and A. Knorr, Phys. Rev. Lett. **91**, 127401 (2003).
[45] A. Krügel, V. M. Axt, T. Kuhn, P. Machnikowski, and A. Vagov, Appl. Phys. B **81**, 897 (2005).
[46] A. Vagov, M. D. Croitoru, V. M. Axt, T. Kuhn, and F. M. Peeters, Phys. Rev. Lett. **98**, 227403 (2007).
[47] A. J. Ramsay, A. V. Gopal, E. M. Gauger, A. Nazir, B. W. Lovett, A. M. Fox, and M. S. Skolnick, Phys. Rev. Lett. **104**, 017402 (2010).
[48] N. Makri and D. E. Makarov, J. Chem. Phys. **102**, 4600 (1995).
[49] N. Makri and D. E. Makarov, J. Chem. Phys. **102**, 4611 (1995).
[50] A. M. Barth, A. Vagov, and V. M. Axt, Phys. Rev. B **94**, 125439 (2016).
[51] J. S. Melinger, D. McMorrow, C. Hillegas, and W. S. Warren, Phys. Rev. A **51**, 3366 (1995).
[52] B. Saleh and M. Teich, *Fundamentals of Photonics, 2 Volume Set*, Wiley Series in Pure and Applied Optics (Wiley Interscience, New York, 2019).
[53] J. P. Reithmaier, G. Sęk, A. Löffler, C. Hofmann, S. Kuhn, S. Reitzenstein, L. V. Keldysh, V. D. Kulakovskii, T. L. Reinecke, and A. Forchel, Nature (London) **432**, 197 (2004).
[54] T. Yoshie, A. Scherer, J. Hendrickson, G. Khitrova, H. M. Gibbs, G. Rupper, C. Ell, O. B. Shchekin, and D. G. Deppe, Nature (London) **432**, 200 (2004).
[55] G. Khitrova, H. M. Gibbs, M. Kira, S. W. Koch, and A. Scherer, Nat. Phys. **2**, 81 (2006).
[56] D. G. Nahri, F. H. A. Mathkoor, and C. H. R. Ooi, J. Phys.: Condens. Matter **29**, 055701 (2017).
[57] K. Kuruma, Y. Ota, M. Kakuda, S. Iwamoto, and Y. Arakawa, Phys. Rev. B **97**, 235448 (2018).
[58] P. Machnikowski and L. Jacak, Phys. Rev. B **69**, 193302 (2004).
[59] A. Krügel, V. M. Axt, and T. Kuhn, Phys. Rev. B **73**, 035302 (2006).
[60] D. Mogilevtsev, A. P. Nisovtsev, S. Kilin, S. B. Cavalcanti, H. S. Brandi, and L. E. Oliveira, Phys. Rev. Lett. **100**, 017401 (2008).
[61] D. Mogilevtsev, A. P. Nisovtsev, S. Kilin, S. B. Cavalcanti, H. S. Brandi, and L. E. Oliveira, J. Phys.: Condens. Matter **21**, 055801 (2009).
[62] A. J. Ramsay, T. M. Godden, S. J. Boyle, E. M. Gauger, A. Nazir, B. W. Lovett, A. M. Fox, and M. S. Skolnick, Phys. Rev. Lett. **105**, 177402 (2010).
[63] D. P. S. McCutcheon and A. Nazir, New J. Phys. **12**, 113042 (2010).
[64] D. P. S. McCutcheon, N. S. Dattani, E. M. Gauger, B. W. Lovett, and A. Nazir, Phys. Rev. B **84**, 081305(R) (2011).
[65] E. R. Schmidgall, P. R. Eastham, and R. T. Phillips, Phys. Rev. B **81**, 195306 (2010).
[66] C.-M. Simon, T. Belhadj, B. Chatel, T. Amand, P. Renucci, A. Lemaitre, O. Krebs, P. A. Dalgarno, R. J. Warburton, X. Marie, and B. Urbaszek, Phys. Rev. Lett. **106**, 166801 (2011).
[67] Y. Wu, I. M. Piper, M. Ediger, P. Brereton, E. R. Schmidgall, P. R. Eastham, M. Hugues, M. Hopkinson, and R. T. Phillips, Phys. Rev. Lett. **106**, 067401 (2011).
[68] S. Lüker, K. Gawarecki, D. E. Reiter, A. Grodecka-Grad, V. M. Axt, P. Machnikowski, and T. Kuhn, Phys. Rev. B **85**, 121302(R) (2012).
[69] K. Gawarecki, S. Lüker, D. E. Reiter, T. Kuhn, M. Glässl, V. M. Axt, A. Grodecka-Grad, and P. Machnikowski, Phys. Rev. B **86**, 235301 (2012).
[70] A. Debnath, C. Meier, B. Chatel, and T. Amand, Phys. Rev. B **86**, 161304(R) (2012).
[71] A. Debnath, C. Meier, B. Chatel, and T. Amand, Phys. Rev. B **88**, 201305(R) (2013).
[72] M. Glässl, A. M. Barth, K. Gawarecki, P. Machnikowski, M. D. Croitoru, S. Lüker, D. E. Reiter, T. Kuhn, and V. M. Axt, Phys. Rev. B **87**, 085303 (2013).
[73] R. Mathew, E. Dilcher, A. Gamouras, A. Ramachandran, Hong Yi Shi Yang, S. Freisem, D. Deppe, and K. C. Hall, Phys. Rev. B **90**, 035316 (2014).
[74] D. E. Reiter, T. Kuhn, M. Glässl, and V. M. Axt, J. Phys.: Condens. Matter **26**, 423203 (2014).
[75] T. Kaldewey, S. Lüker, A. V. Kuhlmann, S. R. Valentin, A. Ludwig, A. D. Wieck, D. E. Reiter, T. Kuhn, and R. J. Warburton, Phys. Rev. B **95**, 161302(R) (2017).
[76] M. Born and V. Fock, Z. Phys. **51**, 165 (1928).
[77] W. M. Itano, J. C. Bergquist, and D. J. Wineland, Phys. Rev. A **38**, 559 (1988).
[78] I. S. Osad'ko, J. Exp. Theor. Phys. **101**, 64 (2005).
[79] X.-Z. Zhang, Z.-H. Wang, H. Li, Q. Wu, B.-Q. Tang, F. Gao, and J.-J. Xu, Chin. Phys. Lett. **25**, 3976 (2008).
[80] J. Sanders, M. Jonckheere, and S. Kokkelmans, Phys. Rev. Lett. **115**, 043002 (2015).